Electronic Supplementary Information

Ionic co-crystals of racetams: Solid-state properties enhancement of neutral active pharmaceutical ingredients via addition of Mg^{2+} and Ca^{2+} chlorides.

Johan Wouters,* Fabrizia Grepioni,* Dario Braga, Saverio Nanna, Baptiste Fours, Gérard Coquerel, Geraldine Longfils, Sandrine Rome, Luc Aerts, and Luc Quéré*

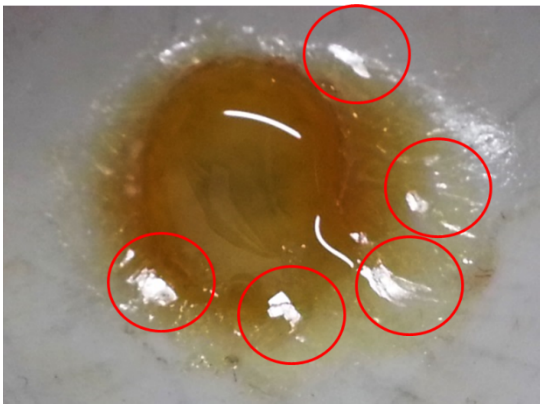

Fig. ESI-1. Single crystals (circled in red) of *BRV*$\cdot CaCl_2\cdot 4H_2O$ (**3**) grown as thin plates from a grinding process followed by addition of a small quantity of water. The crystals are deliquescent.

X-ray powder pattens

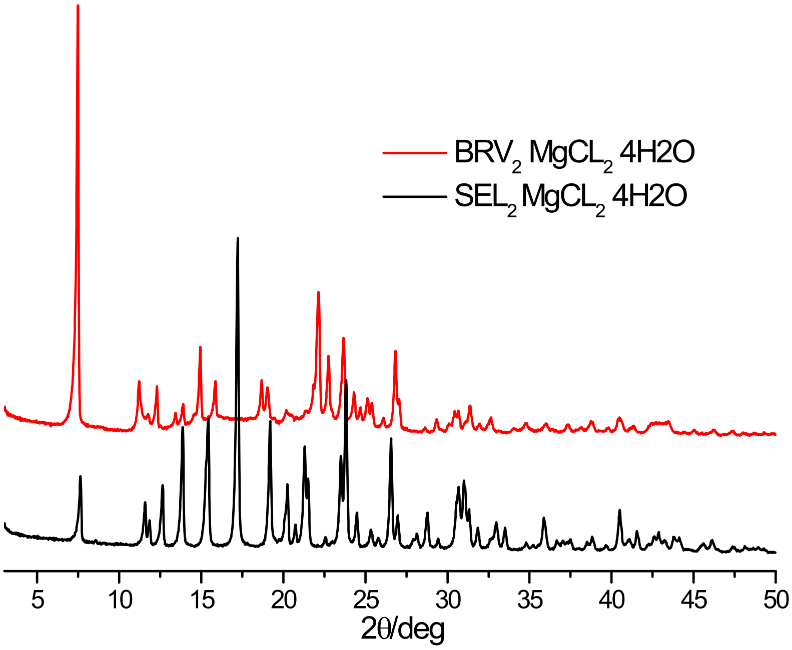

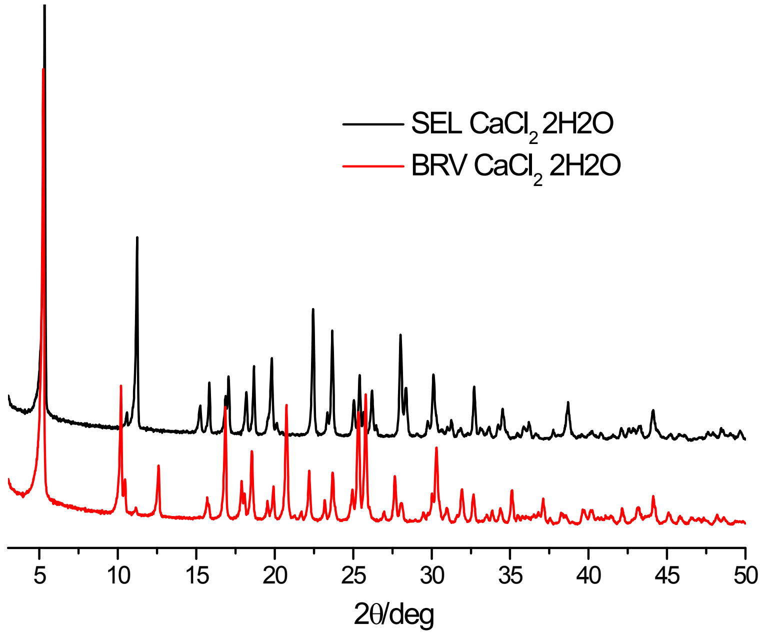

Fig. ESI-XRPD1. X-ray powder patterns for ICCs 1-4 as obtained via kneading with water: (top) XRPD patterns of $BRV_2 \cdot MgCl_2 \cdot 4H_2O$ (red line) and $SEL_2 \cdot MgCl_2 \cdot 4H_2O$ (black line); (bottom) XRPD patterns of $BRV \cdot CaCl_2 \cdot 2H_2O$ (red line) and $SEL \cdot CaCl_2 \cdot 2H_2O$ (black line).

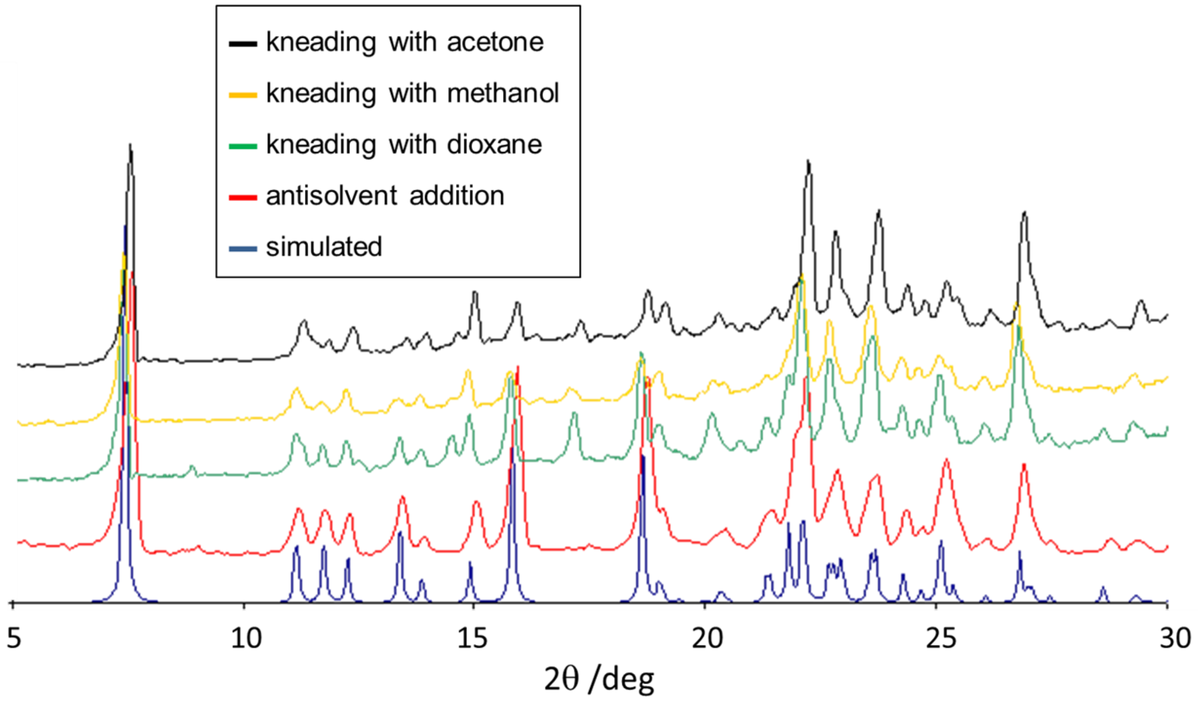

Fig. ESI-XRPD2. Comparison of diffractograms recorded on powder samples of $BRV_2 \cdot MgCl_2 \cdot 4H_2O$ obtained by different crystallization conditions. Diffractograms are compared to the one simulated (bottom) on the basis of the single crystal structure. Note the extra peak at $2\theta = 18°$ corresponding to an excess of hydrated $MgCl_2$ in the sample.

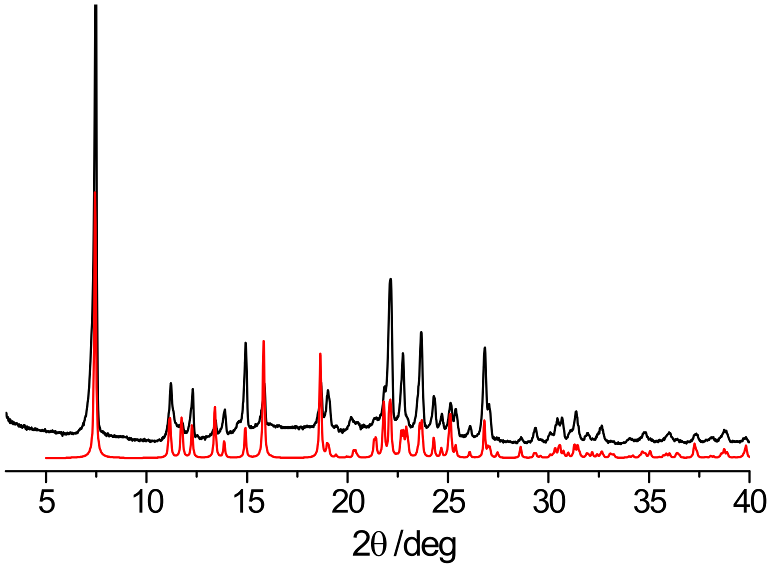

Fig. ESI-XRPD3. Comparison of experimental (black line, powder obtained by the kneading process with water) and calculated (red line, based on single crystal data) powder patterns for *BRV₂*$\cdot MgCl_2 \cdot 4H_2O$.

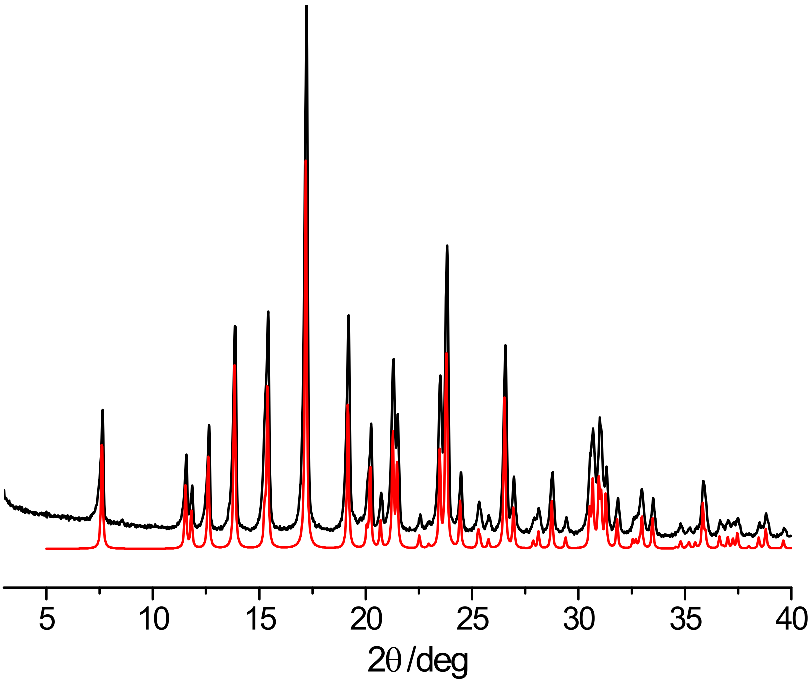

Fig. ESI-XRPD4. Comparison between calculated (red line, single crystal data) and experimental (black line, from ball-milling process) patterns for $SEL_2 \cdot MgCl_2 \cdot 4H_2O$

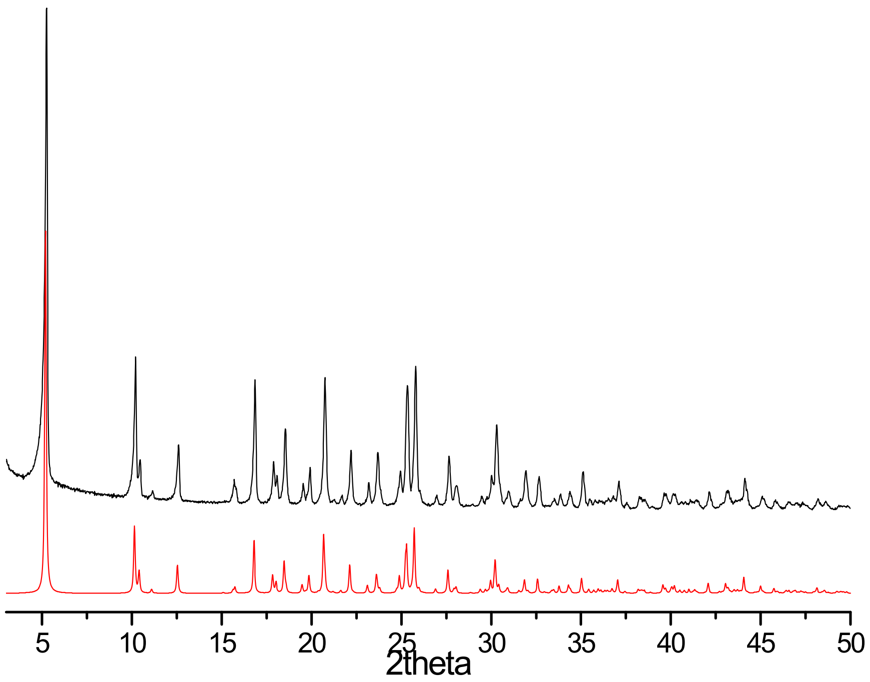

Fig. ESI-XRPD5. Comparison between calculated (red line, powders data) and experimental (black line, from ball-milling process) patterns for BRV·$CaCl_2$·$2H_2O$

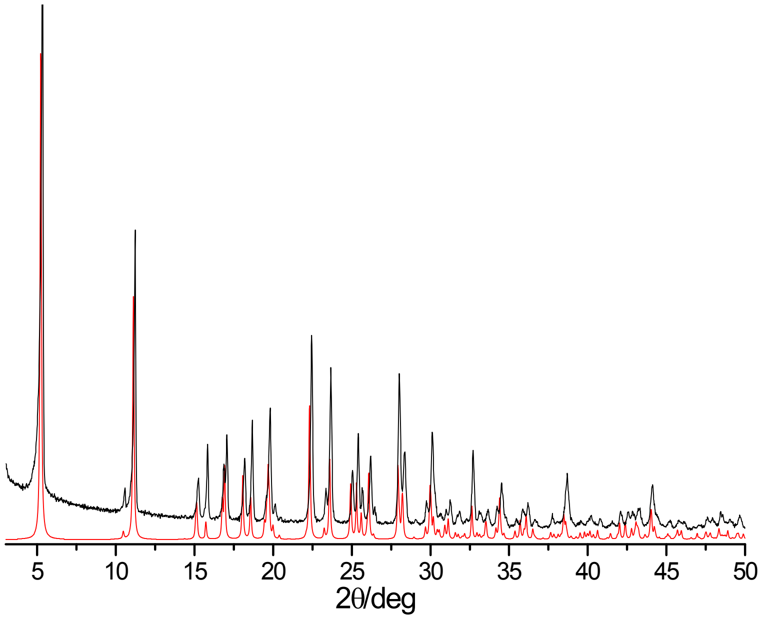

Fig. ESI-XRPD6. Comparison between calculated (red line, single crystal data) and experimental (black line, from ball-milling process) patterns for SEL·$CaCl_2$·$2H_2O$

Structural solution of 3 from powder data

For structure solution and refinement of **3** in the form of a crystalline powder an X-ray powder diffractogram in the 2θ range 3–80° (step size, 0.008°; 0.02 rad soller; kV x mA 40 × 40) was collected on a Panalytical X'Pert PRO automated diffractometer equipped with a X'Celerator detector in Bragg–Brentano geometry and a variable temperature camera Anton Paar TTK450. For phase identification, an X-ray powder diffractogram in the 2θ range 5–50° (step size, 0.0167°; 0.04 rad soller; kV x mA 40 × 40) was collected on a Panalytical X'Pert PRO automated diffractometer in Bragg–Brentano geometry equipped with an X'Celerator detector and a variable temperature camera Anton Paar TTK450. All data were collected using Cu Kα radiation without a monochromator.

The powder XRD pattern of **3** was indexed using DICVOL04,[1] and the space group assigned as $P2_12_12_1$ from systematic absences. Unit cell was determined and profile refinement was conducted using the Pawley profile fitting procedure. Refined unit cell and profile parameters were used for structure solution calculations, via direct-space simulated annealing technique. The best structure solution was used as the initial model for Rietveld refinement; all these operations were carried out using the TOPAS program.[2] For analogy with $SEL\cdot CaCl_2\cdot 2H_2O$ (**4**) we proposed for this co-crystal the formula $BRV\cdot CaCl_2\cdot 2H_2O$. A Pawley on the powder pattern, obtained on the bulk powder from the kneading process, allowed us to calculate an orthorhombic cell, compatible with the presence of one *SEL* molecule, one $CaCl_2$ and two water molecules per formula unit. If the product of the kneading process was left in the air, single crystals were recovered after two days. The quality of single crystals, though not sufficient for a data collection, allowed the determination of the following orthorhombic cell parameters: a = 5.964(7), b = 9.016(1), c = 33.98(3) Å, V.1827(4) Å^3, which are the same, within experimental errors, as the one determined from powder data.

A high resolution powder data collection was carried out, and a structural solution from powder data was attempted in the orthorhombic spage group $P2_12_12_1$ with Z = 4, on the assumption that both stoichiometry and main coordination features are the same in the BRV as in the SEL dihydrated calcium chloride ICC. The model used for the solution (rigid body assumed with only a restricted number of torsional degrees) was taken from the SEL analogue.

1. Boultif, A. and Louer, D. Powder pattern indexing with dichotomy method. *J. Appl. Cryst.* **2004**, 37, 724-731.

2. Bruker-AXS, DIFFRACPlus TOPAS: TOPAS 4.2 Technical Reference, Bruker-AXS GmbH, Karlsruhe, Germany (2008).

Table ESI-1 Selected crystallographic data for **3** (powder data)

Compound reference	**BRV·CaCl$_2$·2H$_2$O (3)** *powder data*
Chemical formula	$C_{11}H_{24}N_2O_4Cl_2Ca$
Formula Mass/g.mol^{-1}	359.30
Crystal system	Orthorhombic
a/Å	5.964(7)
b/Å	9.016(1)
c/Å	33.98(3)
α/°	90
β/°	90
γ/°	90
Unit cell volume/Å^3	1827(4)
Temperature/K	293(2)
Space group	$P2_12_12_1$
No. of formula units per unit cell, *Z*	4

```
#############################################################################

data_BRV_CaCl2*2(H2O)
_chemical_name_systematic     ?
_chemical_name_common     ?
_chemical_formula_moiety     'C11 H20 N2 O2 Ca1 Cl2* 2(H2O)'
_chemical_formula_sum     'C11 H24 N2 O4 Ca1 Cl2'
_chemical_formula_weight     359.3
_chemical_melting_point     ?
_symmetry_cell_setting           orthorhombic
_symmetry_space_group_name_H-M   'P212121'
_symmetry_Int_Tables_number      19
loop_
_symmetry_equiv_pos_as_xyz
 -x,1/2+y,1/2-z
 1/2-x,-y,1/2+z
 x,y,z
 1/2+x,1/2-y,-z
_cell_length_a                34.00986
_cell_length_b                9.01552
_cell_length_c                5.96059
_cell_angle_alpha              90
_cell_angle_beta              90
_cell_angle_gamma               90
_cell_volume                  1827.62
_cell_formula_units_Z     4

_cell_measurement_temperature     295
_exptl_crystal_colour           colourless

_cell_special_details
;
?
```

```
;
_exptl_crystal_density_diffrn    1.306
_exptl_crystal_density_method    'not measured'
_exptl_crystal_F_000    760
_exptl_absorpt_coefficient_mu    5.76
_exptl_special_details
;?
;
_diffrn_ambient_temperature    293
_diffrn_radiation_type    'Cu K\a'
_diffrn_radiation_wavelength    1.54056
_diffrn_radiation_monochromator    'Ge filtered'
_refine_special_details
;
Panalytical X'pert in Debye-Scherrer geometry
;

_computing_data_collection    'Highscore plus'
_computing_cell_refinement       'TOPAS (Coelho ,2007)'
_computing_structure_solution    'TOPAS (Coelho ,2007)'
_computing_structure_refinement    'TOPAS (Coelho ,2007)'

_pd_proc_2theta_range_min    4
_pd_proc_2theta_range_max    50

_pd_proc_info_excluded_regions    'no'
_pd_proc_ls_background_function    'Chebyschev'
_pd_proc_ls_pref_orient_corr
;
Spherical Harmonics
;
_refine_ls_structure_factor_coef Fsqd
_pd_proc_ls_prof_R_factor    0.062
_pd_proc_ls_prof_wR_factor   0.082
_pd_proc_ls_prof_wR_expected    0.019
_refine_ls_number_parameters          152
_refine_ls_goodness_of_fit_all        4.2
_refine_ls_number_restraints          86
_refine_ls_matrix_type               full
_refine_ls_hydrogen_treatment    constr
_pd_spec_mount_mode    reflection
_pd_spec_mounting
;
?
;
_pd_spec_shape    ?


loop_
_atom_site_label
_atom_site_type_symbol
_atom_site_fract_x
_atom_site_fract_y
```

```
_atom_site_fract_z
C8 C 0.914923 -601.7321 469.4336
C9 C 0.86714 -601.9782 469.0897
C10 C 0.8880234 -601.733 469.2278
C11 C 0.864026 -601.5919 469.1842
C12 C 0.8354044 -601.8906 469.4134
C13 C 0.8370936 -602.0984 469.1541
C14 C 0.8110454 -602.0248 469.331
C15 C 0.8497573 -601.586 468.9408
C18 C 0.7731483 -602.2568 469.4445
C21 C 0.8002844 -602.1281 469.5164
N1 N 0.8634058 -601.8647 469.2323
N2 N 0.9268739 -601.6124 469.5381
C55 C 0.7624367 -602.3583 469.6291
Cl1 Cl 1.014286 -602.0882 468.5041
Cl2 Cl 0.9097919 -602.2647 468.4874
Ca1 Ca 0.9459762 -602.0627 468.7488
O1 O 0.8904116 -601.9865 468.9383
O2 O 0.9284064 -601.8467 469.5132
O1W O 0.9829608 -601.9396 469.0279
O2W O 0.9548579 -602.2508 469.0185
H1 H 0.907309 -601.746 469.083
H2 H 0.882365 -601.495 469.218
H3 H 0.838666 -601.591 469.296
H4 H 0.850612 -601.917 469.569
H5 H 0.816679 -601.794 469.439
H6 H 0.851864 -602.195 469.224
H7 H 0.81976 -602.131 469.009
H8 H 0.784289 -601.985 469.251
H9 H 0.831292 -601.682 468.906
H10 H 0.832837 -601.485 468.914
H11 H 0.874991 -601.587 468.828
H12 H 0.788141 -602.321 469.315
H13 H 0.746233 -602.21 469.376
H14 H 0.785333 -602.065 469.646
H15 H 0.827241 -602.175 469.584
H16 H 0.944748 -601.621 469.674
H17 H 0.918255 -601.511 469.483
H18 H 0.747073 -602.297 469.759
H19 H 0.743358 -602.446 469.565
H20 H 0.788981 -602.408 469.699
H21 H 0.99496 -601.849 468.963
H22 H 0.965437 -601.912 469.154
H23 H 0.978943 -602.23 469.107
H24 H 0.931732 -602.254 469.12
###########################################################################
```

Differential scanning calorimetry and thermogravimetric analysis

BRV$_2$·MgCl$_2$·4H$_2$O

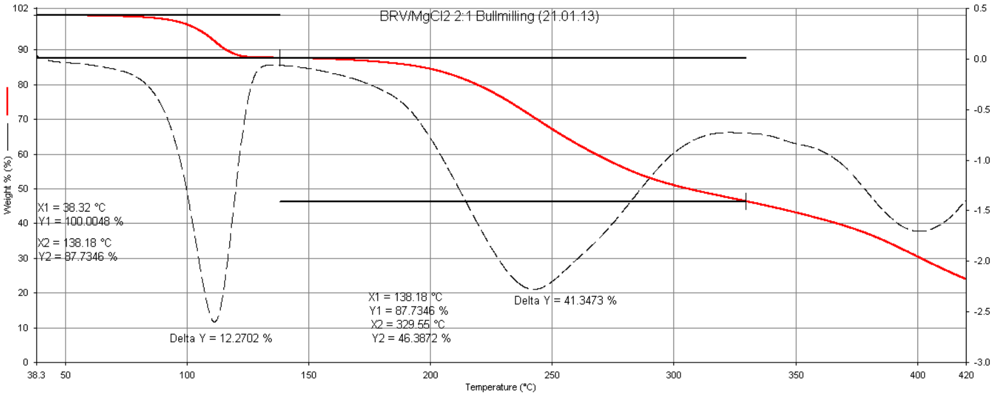

Fig. ESI-TGA1. TGA trace for *BRV*$_2$·MgCl$_2$·4H$_2$O: Water loss is observed in the range 90-120°C, followed by decomposition at ca. 160°C.

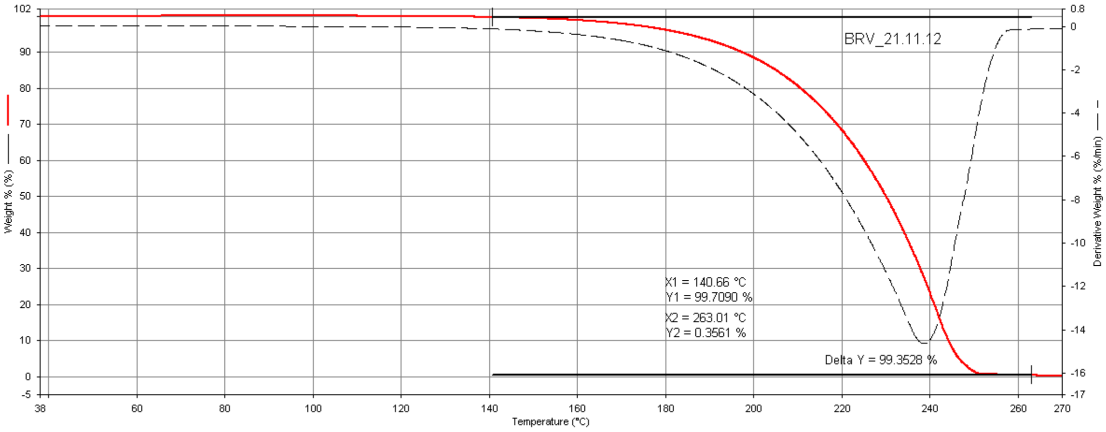

Fig. ESI-TGA2. TGA trace for pure BRV. Decomposition starts at ca. 140°C

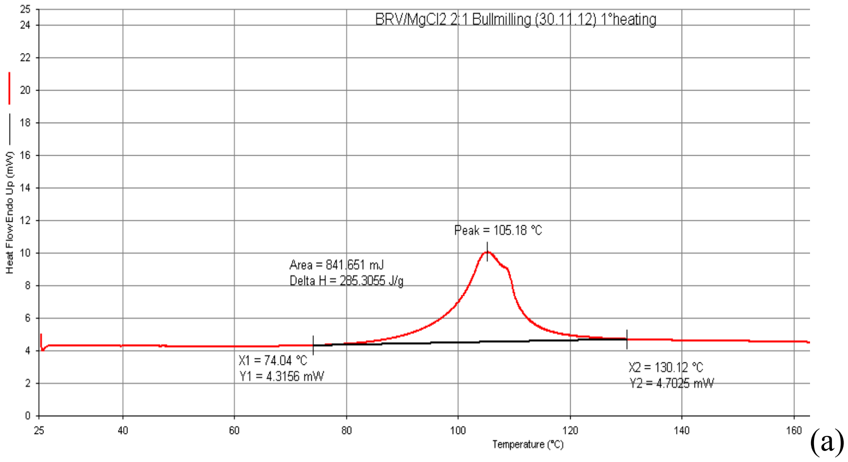

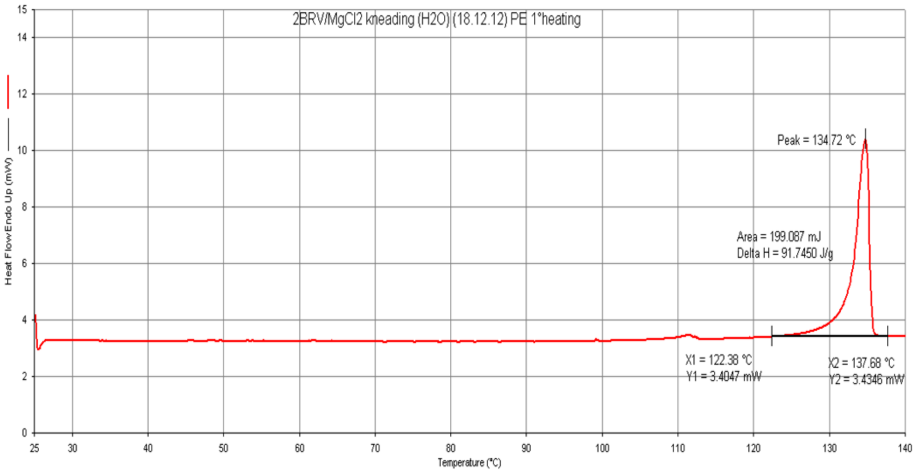

(b)

Fig. ESI-DSC1. (a) Heating cycle (temperature range 25-200°C) for *BRV_2*$\cdot MgCl_2\cdot 4H_2O$ in an open pan; (b) heating cycle (temperature range 25-140°C) in a sealed pan.

$\boldsymbol{SEL_2\cdot MgCl_2\cdot 4H_2O}$

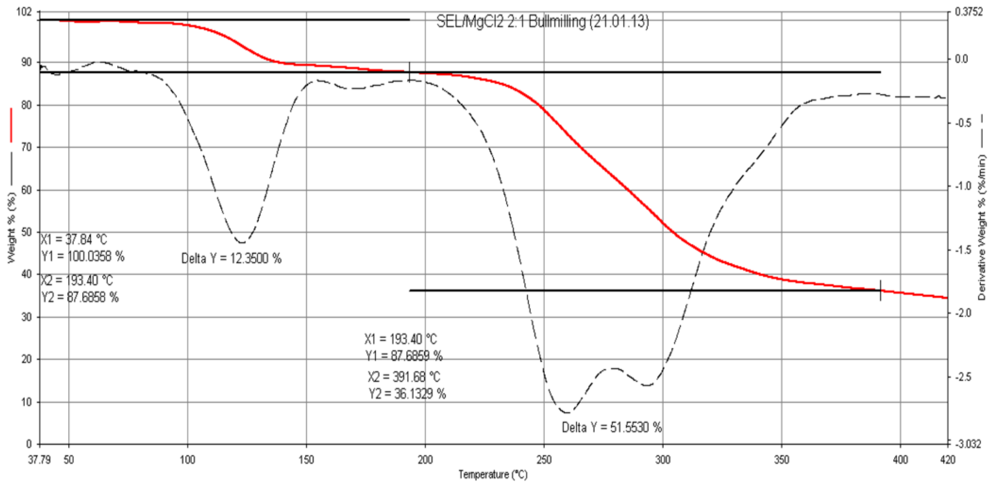

Fig. ESI-TGA3. TGA trace for *SEL_2*$\cdot MgCl_2\cdot 4H_2O$: Water loss is observed in the range 90-150°C, followed by decomposition at ca. 200°C.

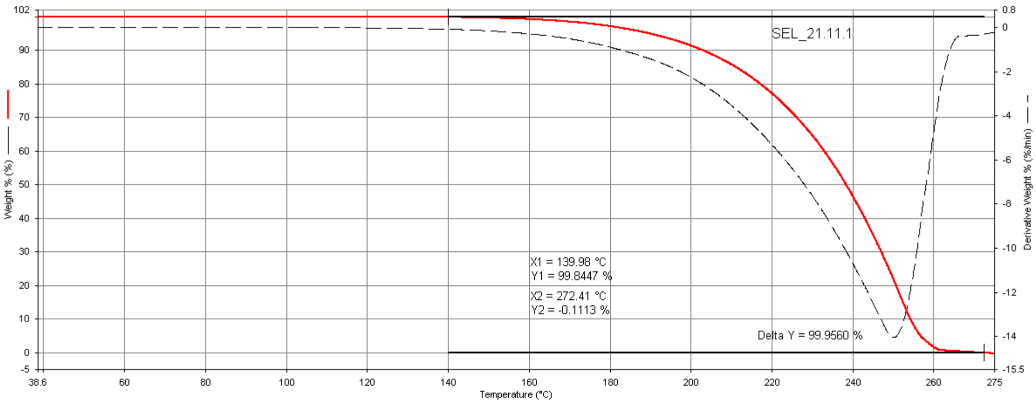

Fig. ESI-TGA4. TGA trace for pure SEL. Decomposition starts at ca. 140°C

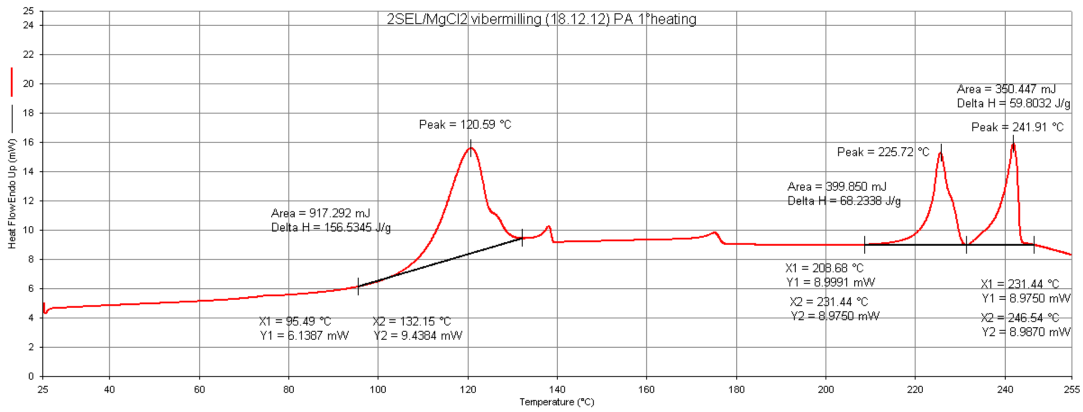

Fig. ESI-DSC2a. DSC in open pan - Heating cycle: loss of water in the range 100-130 °C (peak at 120 °C); melting accompanied by decomposition is observed above 200 °C.

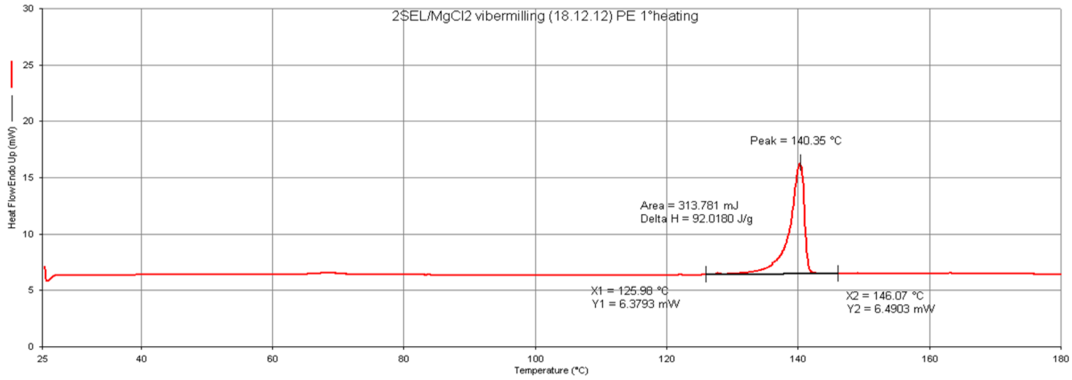

Fig. ESI-DSC2b. DSC in sealed pan - Congruent melting (as observed at UCB) of the hydrated form is observed at ca. 140 °C; no recrystallization is observed on cooling.

BRV·$\mathbf{CaCl_2{\cdot}2H_2O}$

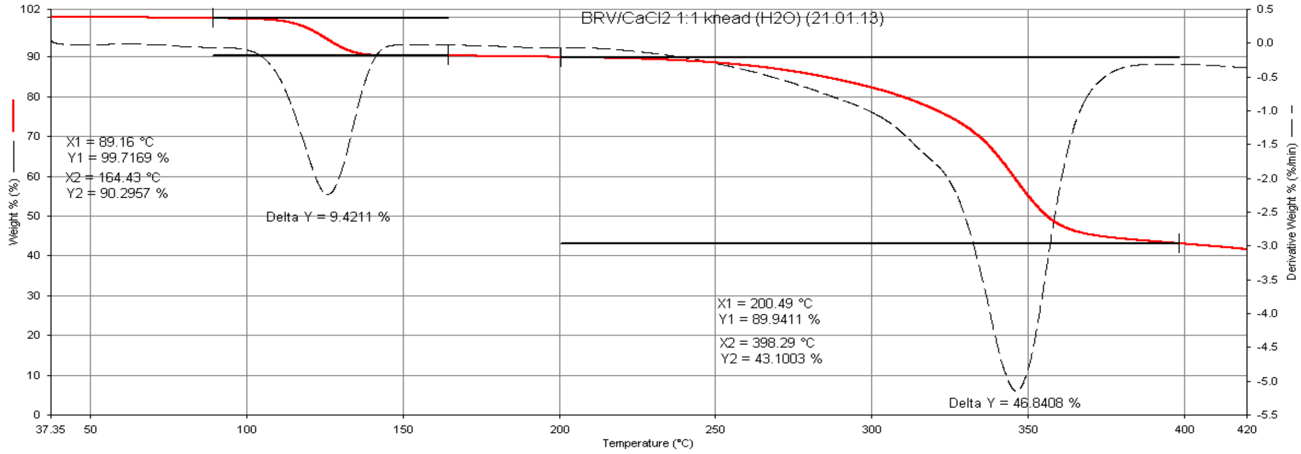

Fig. ESI-TGA5. Mass loss (9.4%) between 100 and 140°C, (this corresponds to the loss of two water molecules, if we assume that the formula is BRV·$CaCl_2$·$2H_2O$); decomposition starts at ca. 200°C.

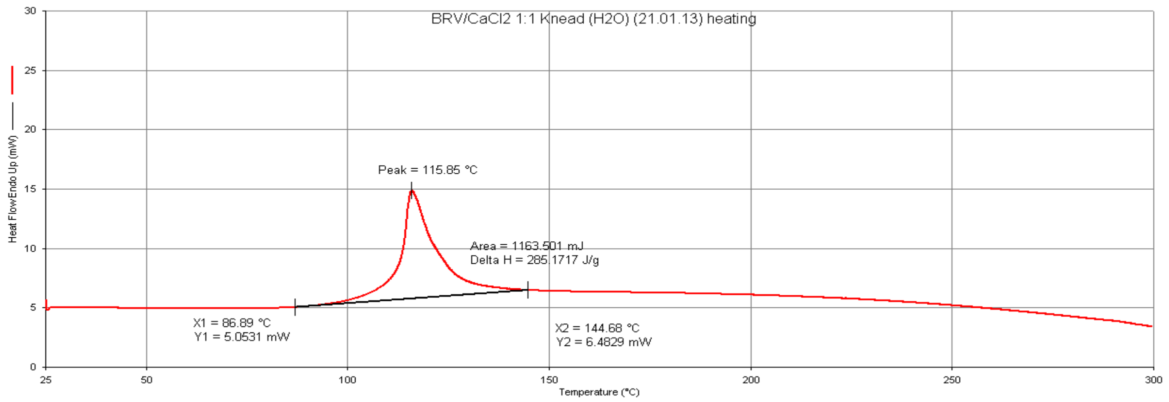

Fig. ESI-DSC3a. DSC in open pan. 1st Heating cycle: at 115.9°C (peak) an endothermic event, *due to loss of water followed by melting* - is observed (ΔH 285 J g^{-1}). The baseline changes starting from ca. 200°C (decomposition).

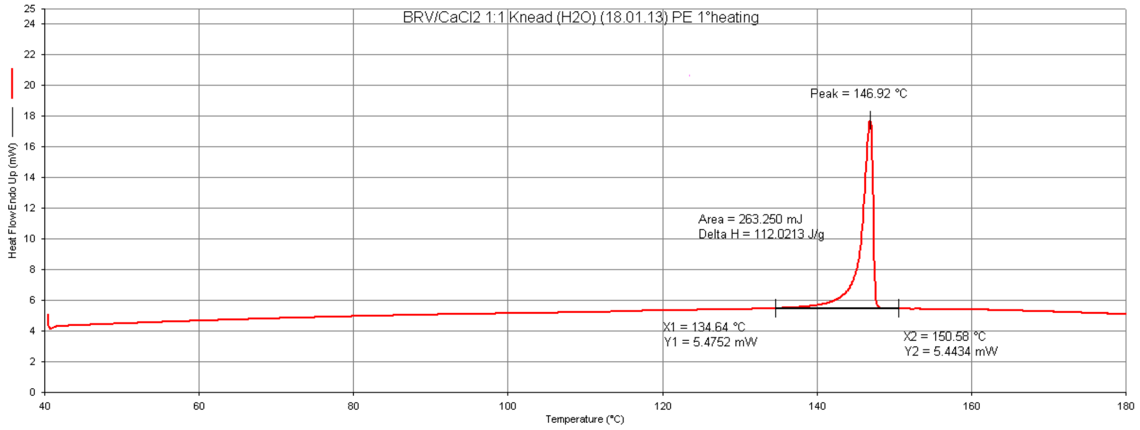

Fig. ESI-DSC3b. DSC in sealed pan.

SEL$\cdot$CaCl$_2\cdot$2H$_2$O

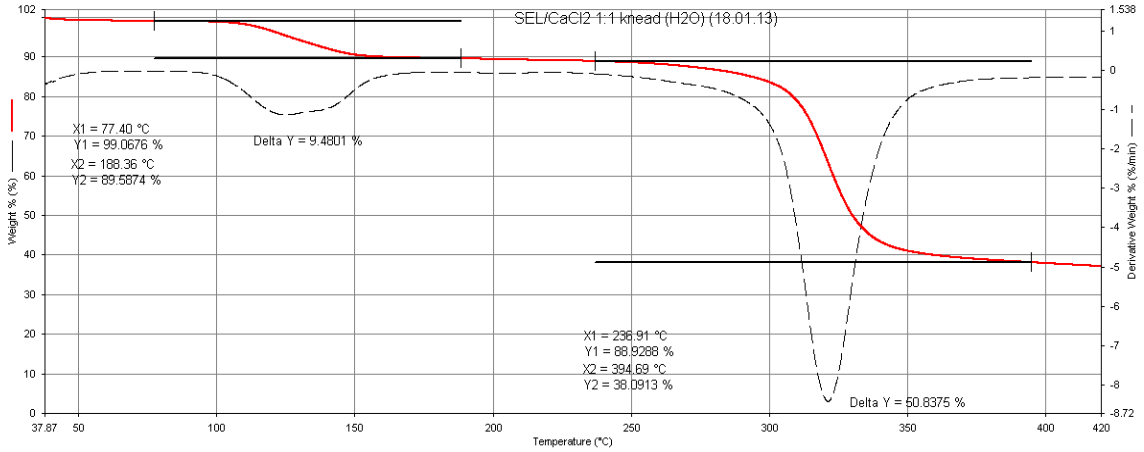

Fig. ESI-TGA6. *SEL*·CaCl$_2$·2H$_2$O. Mass loss due to dehydration (9.5%) in the range 100-150°C; decomposition starts at ca. 250°C.

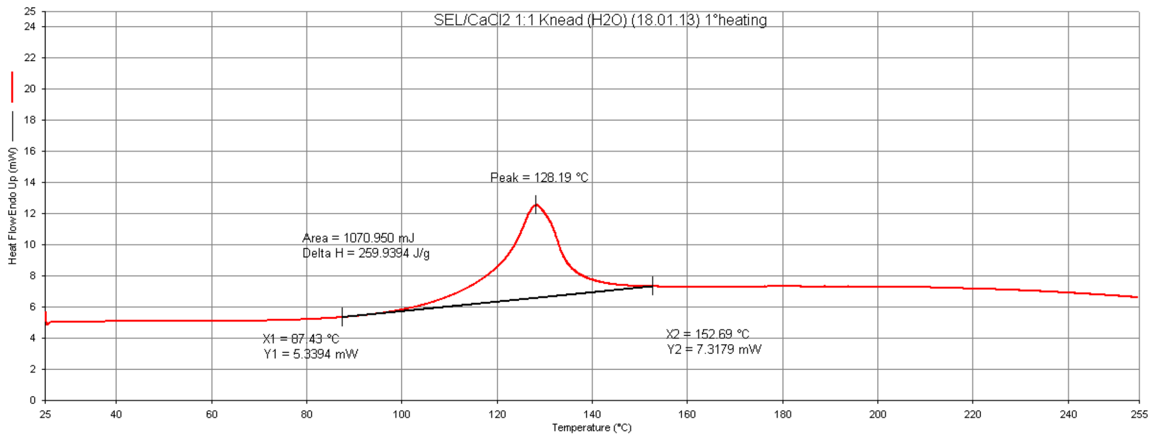

Fig. ESI-DSC4a DSC in open pan. Heating cycle: at 128 °C (peak temperature; 260 J g^{-1}) a broad endothermic peak is observed.

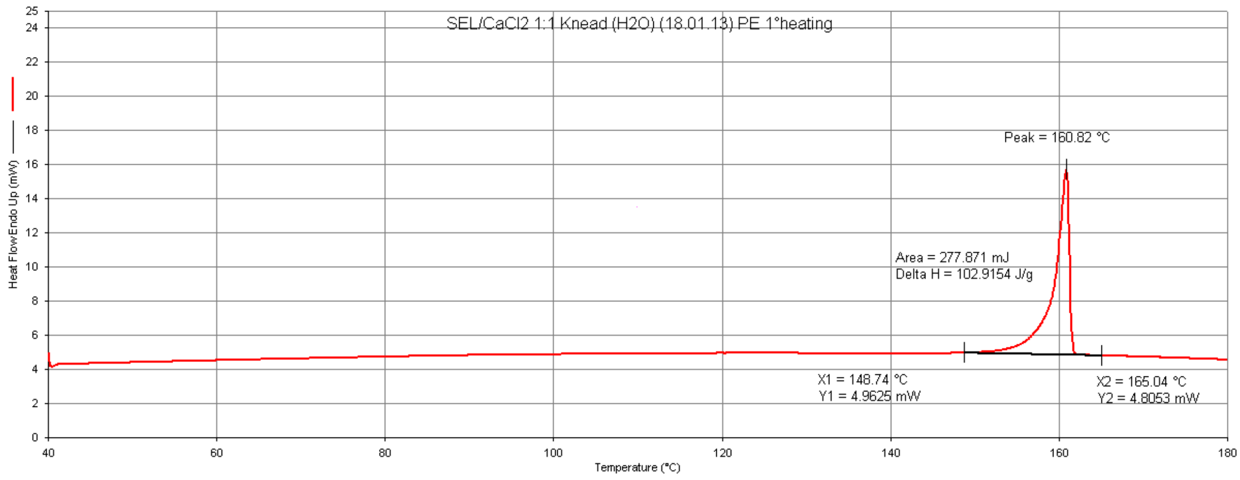

Fig. ESI-DSC4b. *SEL*$\cdot$CaCl$_2\cdot$2H$_2$O, **DSC in sealed pan.**

Hot-stage microscopy with polarized light (HSM)

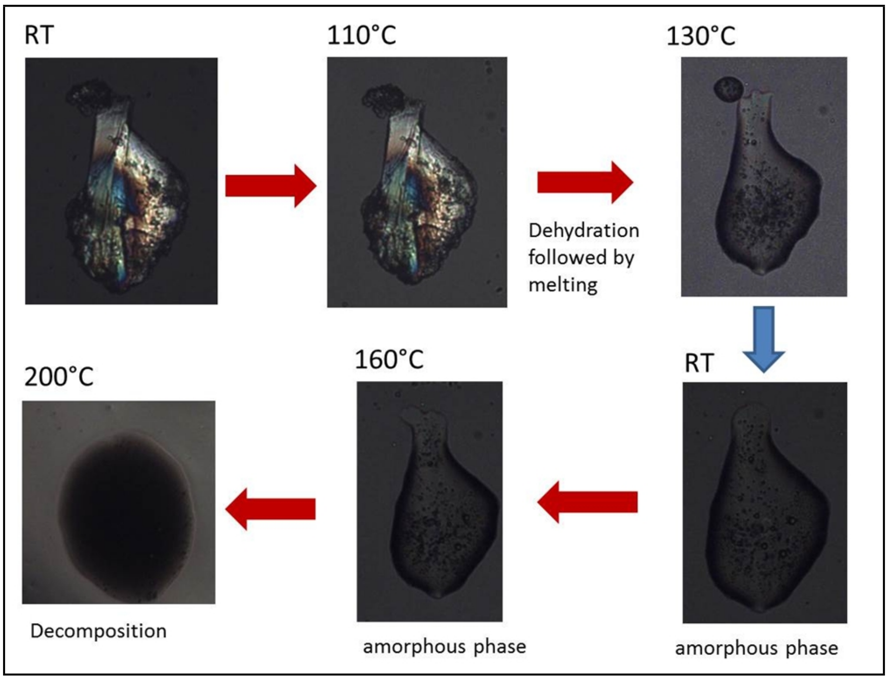

Fig. ESI-HSM1. Single crystal of *BRV₂*$\cdot MgCl_2\cdot 4H_2O$. Heating and cooling processes (both at 5°C min^{-1}) are indicated by red and blue arrows, respectively.

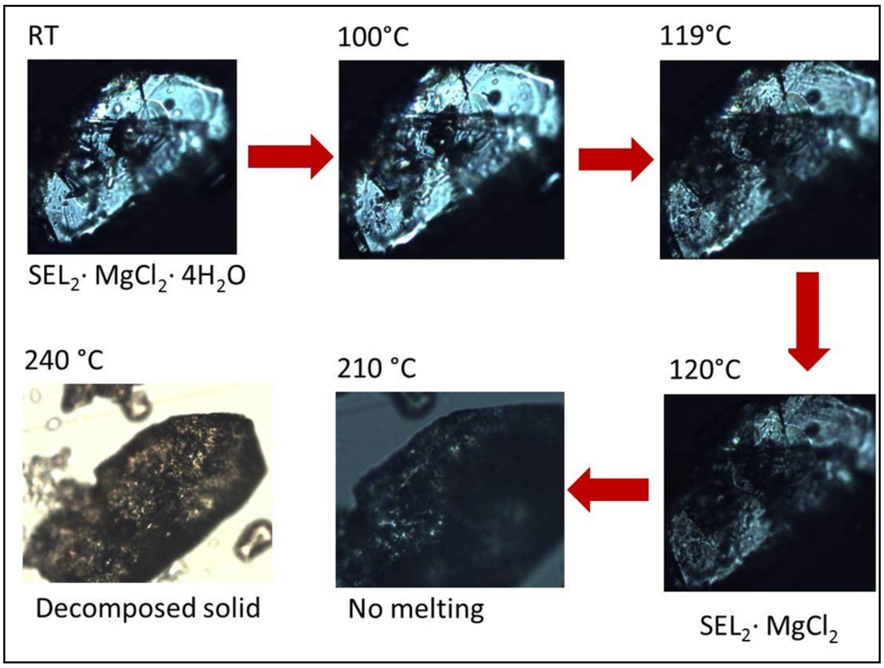

Fig. ESI-HSM2. HSM on a single crystal of $SEL_2\cdot MgCl_2\cdot 4H_2O$ (heating 1 - 10°C/min). Loss of water is observed at ca. 120°C, accompanied by formation of a polycrystalline/amorphous solid. No melting can be detected at higher temperature; at 240°C the solid is decomposed (“burnt”-like solid

– picture taken without polaryzer). The observations are in agreement with TGA and, on the whole, with DSC in open pan.

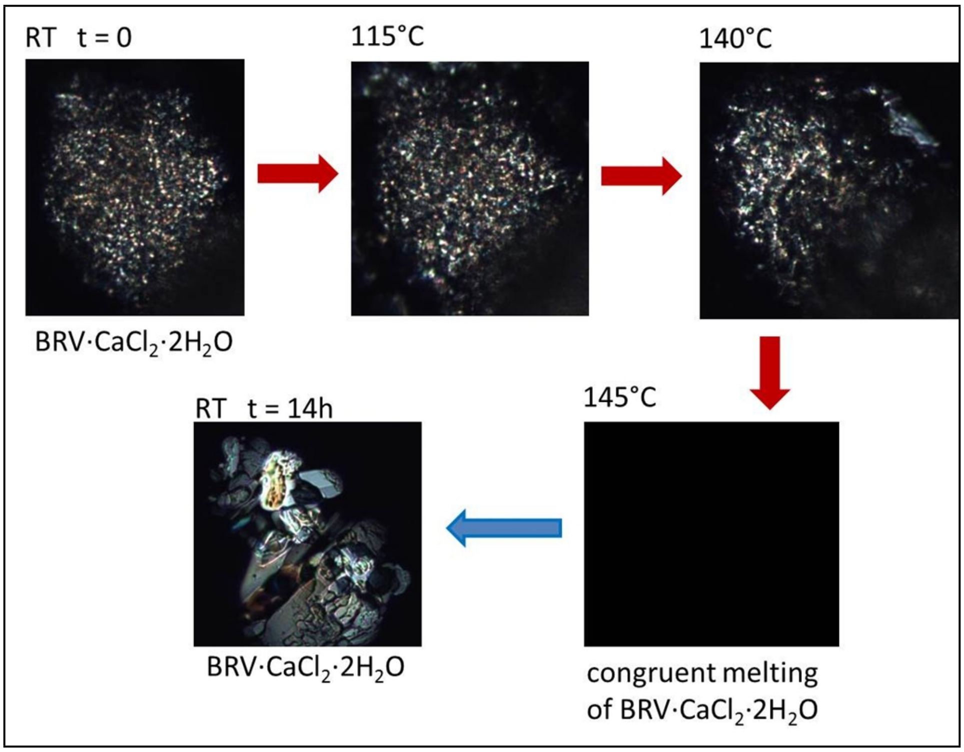

Fig. ESI-HSM3. Crystalline powder of ***BRV*·$CaCl_2$·$2H_2O$** (heating rate 5°C min^{-1}). Congruent melting of the hydrated phase is observed starting at 140°C; the melting process is complete at 145°C, as observed in the DSC trace (sealed pan). If the sample is left in the air, recrystallization of the hydrated form is observed.

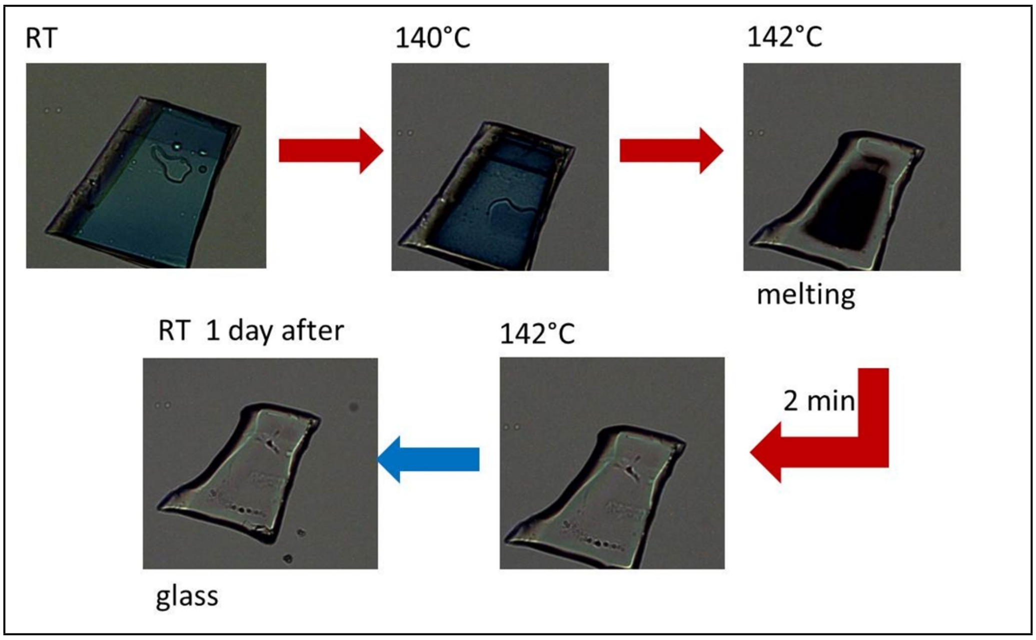

Fig. ESI-HSM4. HSM on a single crystal of *SEL*·$CaCl_2$·$2H_2O$. The beahviour is analogous to the one observed for the polycrystalline material, although the melting is observed here at higher temperature (but still in the T range of open pan DSC). (Heating rate 5 °C min^{-1}, cooling rate 10°C min^{-1})

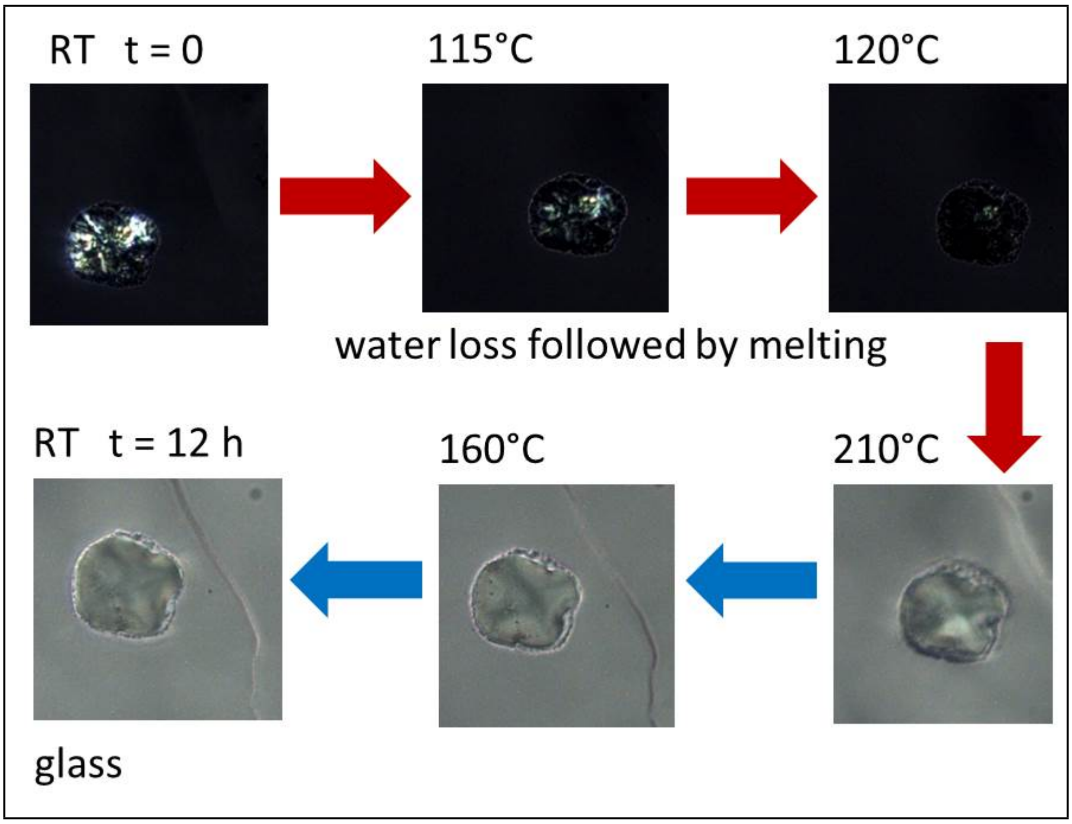

Fig. ESI-HSM5. HSM on a polycrystalline sample of *SEL*·$CaCl_2$·$2H_2O$. Amorphization/melting due to water loss is observed in the 115-120°C range, as in the DSC trace (open pan). Polarization effect has been reduced for the images on cooling, to show how the sample remains amorphous (glassy state). (Heating rate 5 °C min^{-1}, cooling rate 2°C min^{-1})

Variable temperature X-ray powder diffraction(VTXRPD)

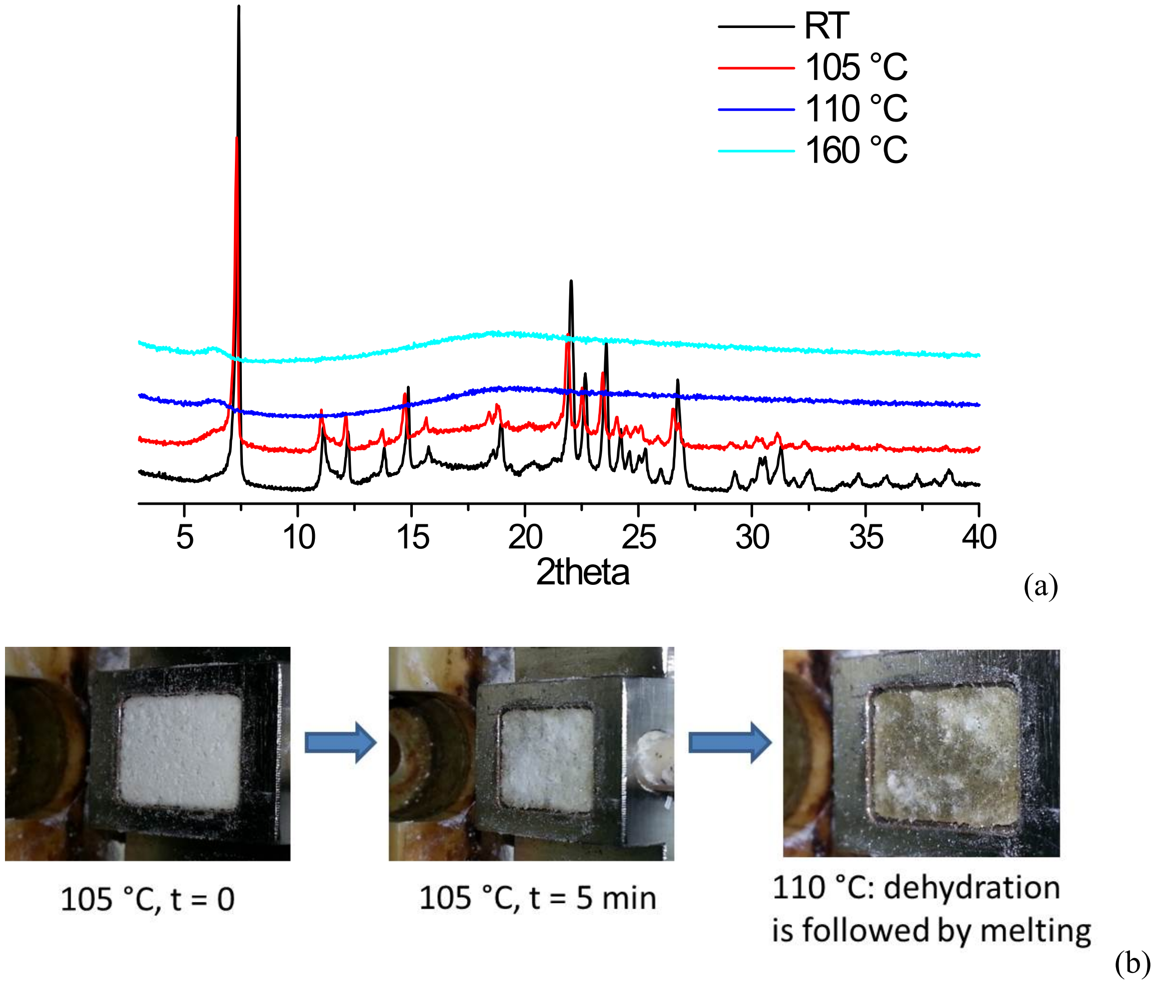

105 °C, t = 0

105 °C, t = 5 min

110 °C: dehydration is followed by melting

Fig. ESI-VTXRPD1. (a) VT-XRPD measurements on a *BRV*$_2$·$MgCl_2$·$4H_2O$ sample obtained via kneading. A decrease in crystallinity can be detected at 105°C, while at 110°C complete amorphization of the sample is observed. The heating process was stopped at 160°C, to avoid decomposition; the sample does not recrystallize upon cooling down to RT. (b) Pictures of the sample, taken during the VT-XRPD measurement, at the dehydration and melting stages.

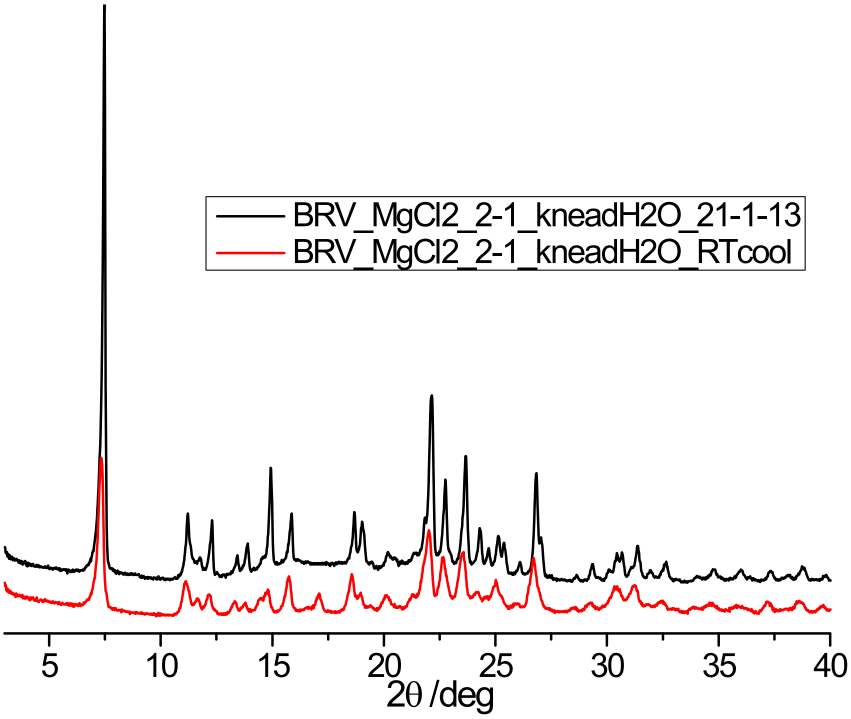

Fig. ESI-VTXRPD2. Comparison between the X-ray powder pattern measured on *BRV*$_2$·MgCl$_2$·4H$_2$O after cooling back to RT (red line) and that obtained with the kneading process (black line); thepeak at ca. 17 deg in the red pattern is due to traces of unreacted BRV.

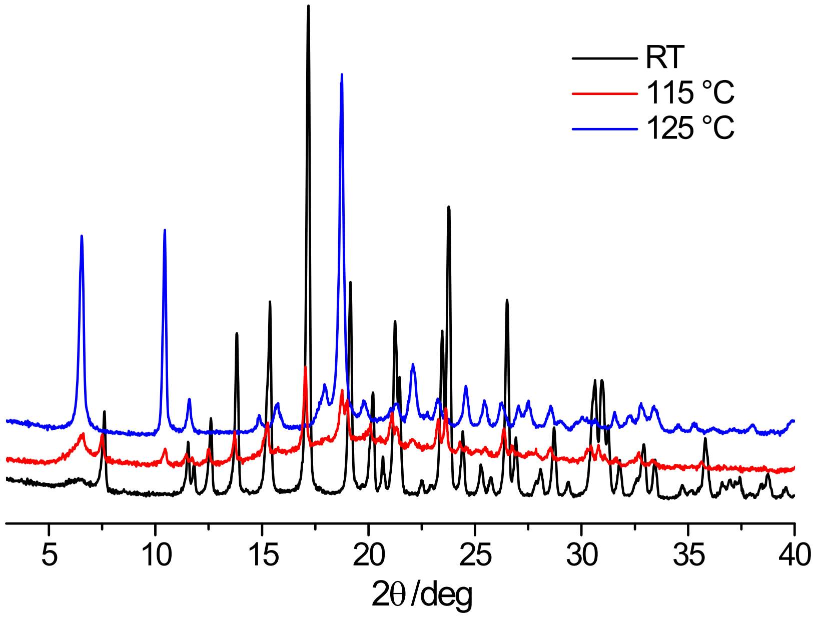

(a)

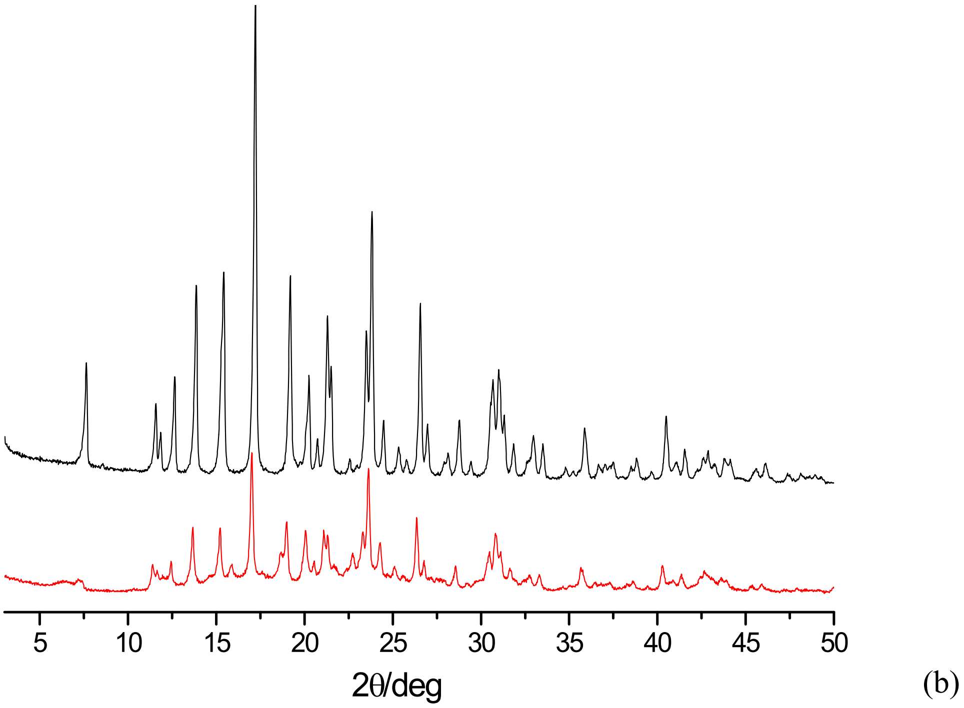

Fig. ESI-VTXRPD3. (a) VT-XRPD measurements on *SEL*$_2$·MgCl$_2$·4H$_2$O sample obtained via ball-milling (black line). A decrease in crystallinity can be detected at 115°C, together with the appearace of new peaks (red line); at 125°C complete transformation is observed to a new, possibly anhydrous but unstable form (blue line). (b) Comparison between the X-ray powder pattern measured at RT on *SEL*$_2$·MgCl$_2$·4H$_2$O, 2 hours after the VTXRPD measurements of Fig. ESI-VTXRPD3 (red line) and that obtained via ball milling (black line). Conversion back to the hydrated form is almost complete.

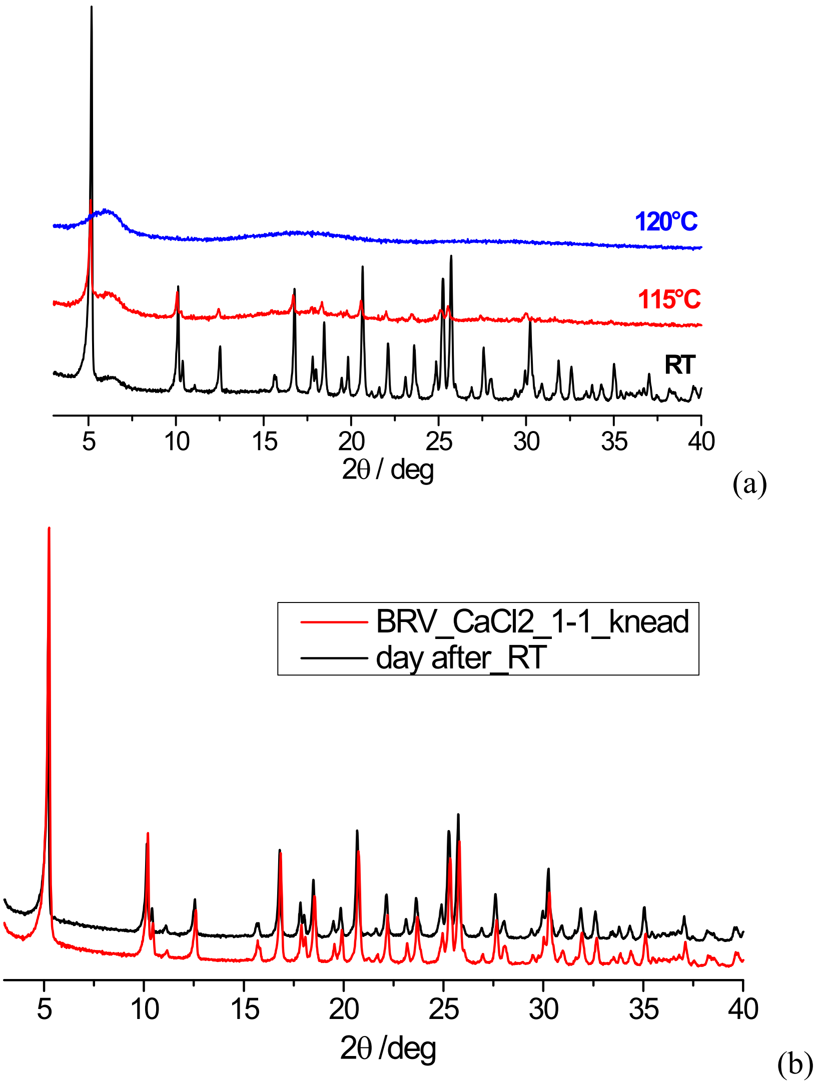

Fig. ESI-VTXRPD4. (a) VT-XRPD measurements on crystalline *BRV*·$CaCl_2$·$2H_2O$ (black line). A decrease in crystallinity can be detected at 115°C; at 125°C complete amorphization of the sample is observed, which follows the dehydration process. If the sample is left in the air for 24h, water is absorbed from the atmosphere and the crystalline, hydrated phase *BRV*·$CaCl_2$·$2H_2O$ is reobtained (see next figure)

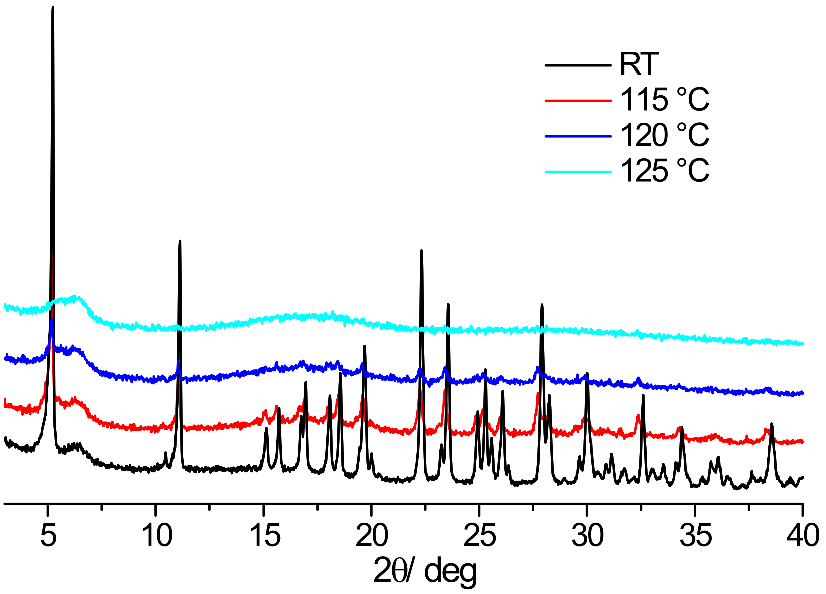

(a)

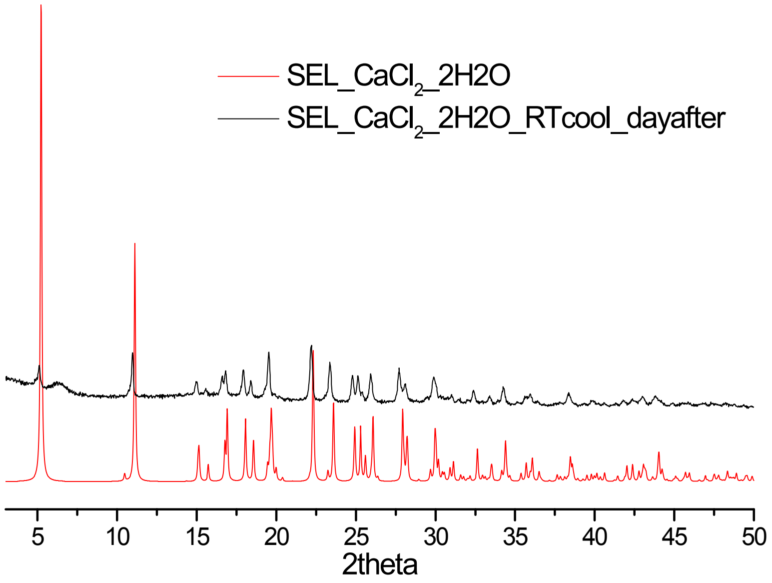

(b)

Fig. ESI-VTXRPD5. (a) VT-XRPD measurements on crystalline *SEL*·$CaCl_2$·$2H_2O$ (black line). Dehydration starts at ca. 115°C (lowering of peaks intensity), immediately followed by formation of an amorphous phase; at 125°C the process is complete. (b) If the sample is left in the air for 12h, water is absorbed from the atmosphere and the crystalline, hydrated phase *SEL*·$CaCl_2$·$2H_2O$ is reobtained.